PERGAMON

International Journal of Solids and Structures 38 (2001) 4045–4069

INTERNATIONAL JOURNAL OF SOLIDS and STRUCTURES

www.elsevier.com/locate/ijsolstr

Effective elastoplastic behavior of ductile matrix composites containing randomly located aligned circular fibers

J.W. Ju *, X.D. Zhang [1]

Department of Civil and Environmental Engineering, University of California at Los Angeles, 5731/5732 Boelter Hall, P.O. Box 951593, Los Angeles, CA 90095-1593, USA

Received 3 March 1999; in revised form 20 May 2000

Abstract

Based on the micromechanical framework and the second-order transverse effective elastic moduli of fiber-reinforced composites derived by Ju and Zhang [Int. J. Solids Struct. 35 (1998) 941], effective elasto-(visco-)plastic behavior of two-phase unidirectional fiber-reinforced ductile matrix composites (FRDMCs) is studied in detail. The circular fibers are assumed to be elastic and unidirectionally aligned while the matrix phase can be either elastic or plastic, depending on the local stress state and effective yield criteria. Furthermore, the ensemble-averaged stress norm is constructed based on the probabilistic distribution of circular fibers, pairwise fiber interactions and the ensemble-area averaging procedure. Together with the plastic flow rule and hardening law postulated in continuum plasticity, the aforementioned stress norm is employed to characterize the overall yield criteria which determine the elastoplastic behavior of FRDMCs under general transverse plane-strain loading and unloading histories. As a special case, the initial effective yield criteria for incompressible ductile matrix containing many unidirectionally aligned cylindrical voids are also derived. In addition, the overall elasto-viscoplastic behavior of FRDMCs is investigated based on the Duvaut–Lions viscoplasticity. Finally, comparison between our theoretical predictions and the available experimental data for FRDMCs is performed to illustrate the capability of the proposed framework.

Keywords: Ductile matrix composites; Randomly located fibers; Aligned circular fibers; Effective elastoplasticity; Micromechanics of composites

1. Introduction

The improvement in processing and manufacturing technology during recent years facilitates the production of advanced composite materials, including the fiber-reinforced ductile matrix composites (FRDMCs). The matrix materials of the FRDMCs are made of ductile metals or alloys (such as aluminum, steel or titanium) with high strain capability, whereas the fibers behave elastically (such as the carbon, boron or glass fibers). Once FRDMCs are loaded beyond the effective yield points, the overall elastoplastic

* Corresponding author. Tel.: +1-310-206-1751; fax: +1-310-206-2222.
E-mail address: juj@ucla.edu (J.W. Ju).
[1] Present address: Ford Motor Company, Detroit M148141, USA.

0020-7683/01/$ - see front matter
PII: S0020-7683(00)00270-5

response will follow. The optimal microstructural design of FRDMCs enables the stiffness enhancement within the elastic range and the ductility and strength control within the plastic range. Therefore, it is desirable to characterize and predict the elastoplastic behavior of FRDMCs. Although engineers can control the manufacturing of periodic fiber array in FRDMCs with large-diameter fibers, it is difficult and expensive to achieve periodic fiber distribution with small-diameter fibers (e.g., carbon or glass fibers). The present study investigates the overall elastoplastic behavior of FRDMCs with unidirectionally aligned yet randomly located circular fibers. FRDMCs offer highly directional properties such as high specific stiffnesses along the fiber direction. However, the elastic and elastoplastic properties along the transverse direction are also an important research topic.

Extensive theoretical methods exist in the literature to predict overall elastic moduli of fiber reinforced composites. See, for example, Hill (1963, 1964a), Hashin (1972, 1983), Willis (1981, 1982), Mura (1987), Zhao and Weng (1990a), Nemat-Nasser and Hori (1993), and Ju and Zhang (1998) for more details. By adopting the overall elastic moduli of fiber reinforced composites with transversely isotropic phases (Hill, 1964a,b) first incorporated the plastic flow theory to evaluate the elastoplastic incremental moduli of FRDMCs. Adams (1970) utilized a finite element analysis together with classical Prandtl–Reuss flow rule to predict the inelastic behavior of unidirectional composite under transverse normal loading. Lin et al. (1972a) studied the initial yield surfaces of unidirectional B/Al composites subjected to combined longitudinal normal, transverse normal, and in-plane longitudinal shear loadings. Subsequent study (Lin et al., 1972b) indicated that the yielding initiated at opposite corners of the fiber–matrix interface closest to adjacent fibers, and that the plastic zone expanded very fast in the matrix with increasing applied loads.

Hashin (1980) proposed three-dimensional failure criteria for unidirectional fiber composites by considering four distinct failure modes, resulting in a piecewise smooth failure surface. Dvorak and Bahei-El-Din (1987) predicted the shape and position of yield surface with the bimodal plasticity theory. Further, experimental study and comparison with the bimodal theory were presented by Dvorak et al. (1988) and Dvorak (1991). Based on the Mori–Tanaka method (Mori and Tanaka, 1973) and the framework by Tandon and Weng (1988), Zhao and Weng (1990b) derived a multiaxial theory of plasticity for a class of composites containing unidirectionally aligned spheroidal inclusions, including unidirectional fibers as a special case. DeBotton and Ponte Castañeda (1993) employed a procedure proposed by Ponte Castañeda (1991, 1992) to obtain both estimates and rigorous bounds for the effective energy functions of fiber-reinforced composites with general ductile behavior. More recently, Ju and Chen (1994a) proposed a micromechanical framework to predict the effective elastoplastic behavior of two-phase metal matrix composites under general loading/unloading histories by considering the *first-order* stress perturbations of elastic particles to the ductile matrix. Ju and Tseng (1996, 1997) further improved the foregoing work by incorporating the second-order stress perturbations due to pairwise particle interactions, following the work of Ju and Chen (1994b,c).

In accordance with the plasticity theory, every *local* matrix point has its own plastic field quantities (such as plastic strains and plastic hardening variables). For a statistically homogeneous ductile matrix composite containing randomly located yet unidirectionally aligned fibers, the Monte Carlo method would require hundreds of simulations in order to obtain pointwise elastoplastic response under specified loading history. Further, statistical averaging of Monte Carlo simulations would need to be performed to render a statistically homogenized (overall) elastoplastic response. This method is impractical owing to the complexity of random microstructure and the tremendous computational effort. An attractive alternative is to employ the ensemble-volume averaging method at the micromechanical level. In the present study, the ''local stress norm'' is analytically derived for the matrix plasticity formulation by a micromechanical approach which considers complete *second-order* pairwise inter-fiber interactions for *both* the elastic and plastic sub-problems. Probabilistic ensemble average is subsequently applied to obtain a homogenized plastic yield function. In addition, the plastic flow rule and hardening law are then postulated at the composite level based on

continuum plasticity. Therefore, complete *second-order* macroscopic effective elastoplastic constitutive models are constructed for FRDMCs.

The main objective of this paper is to predict effective elastoplastic behavior of two-phase FRDMCs based on mechanical properties of the constituent phases, volume fractions, random spatial distributions and micro-geometries of the fibers. Furthermore, the fibers are assumed to be *elastic* circular cylinders (randomly located yet unidirectionally aligned), and the ductile matrix behaves *elastoplastically* under general loading histories. All fibers are assumed to be nonintersecting and embedded firmly in the matrix with perfect interfaces.

This paper is organized as follows. In Section 2, effective elastic moduli of two-phase FRDMCs are summarized based on Ju and Zhang (1998). A second-order formulation is presented in Section 3 to account for fiber interaction effects. A unified formulation is proposed to derive the overall yield functions for both fibrous and porous composites. In addition, the plastic flow rule and hardening law are postulated according to continuum plasticity to characterize the plastic behavior under *general* one-dimensional loading and unloading histories (in contrast to monotonic and proportional loadings assumed by many existing works in the micromechanics literature). Initial effective yield criteria for incompressible ductile matrix containing many unidirectionally aligned cylindrical voids are presented in Section 4. Furthermore, in Section 5, plane-strain transverse elastoplastic stress–strain behavior of FRDMCs is studied for both uniaxial and biaxial loading conditions. Comparison between our analytical prediction and available experimental data is also illustrated. Finally, the initial yield surfaces of FRDMCs and viscoplastic extension are derived in Sections 6 and 7, respectively.

2. Effective elastic moduli of two-phase composites containing randomly located aligned circular fibers

Following the notation in Ju and Zhang (1998), a two-phase composite consists of an elastic matrix (phase 0) and unidirectionally aligned, infinitely long and randomly located elastic circular fibers (phase 1) with distinct material properties. The two phases are assumed to be perfectly bonded at interfaces. Furthermore, the composite is assumed to be in a plane-strain state throughout this paper. The relation between the stress $\boldsymbol{\sigma}$ and strain $\boldsymbol{\epsilon}$ at any point $\mathbf{x}$ in the α-phase ($\alpha = 0$ or 1) are governed by

$$\boldsymbol{\sigma}(\mathbf{x}) = \mathbf{C}_\alpha : \boldsymbol{\epsilon}(\mathbf{x}), \tag{1}$$

where ":" denotes the tensor contraction and $\mathbf{C}_\alpha$ is the plane-strain linearly elastic stiffness tensor. At the macroscopic level, the overall plane-strain elastic stiffness tensor $\mathbf{C}_*$ is defined as the relation between overall averages of stress and strain:

$$\bar{\boldsymbol{\sigma}} = \mathbf{C}_* : \bar{\boldsymbol{\epsilon}}. \tag{2}$$

2.1. Inter-fiber interactions and ensemble-area averaged fields

In Ju and Zhang (1998), it was shown that the approximate ensemble-area averaged eigenstrain $\langle \bar{\boldsymbol{\epsilon}}^* \rangle$ (accounting for *pairwise* plane-strain fiber interaction) is related to the *noninteracting* eigenstrain solution $\boldsymbol{\epsilon}^{*0}$ as follows

$$\langle \bar{\boldsymbol{\epsilon}}^* \rangle = \Gamma : \boldsymbol{\epsilon}^{*0}, \tag{3}$$

where the components of the *isotropic* tensor Γ are defined as

$$\Gamma_{ijkl} = \gamma_1 \delta_{ij}\delta_{kl} + \gamma_2(\delta_{ik}\delta_{jl} + \delta_{il}\delta_{jk}) \tag{4}$$

in which (assuming the uniform "radial distribution function" throughout this paper; cf. Ju and Zhang, 1998; Batchelor and Green, 1972; Willis and Acton, 1976; Chen and Acrivos, 1978)

$$\gamma_1 = \frac{\phi}{4\beta^2}\left[-2 + \frac{\beta(1-2\nu_0)}{\alpha+\beta}\right], \tag{5}$$

$$\gamma_2 = \frac{1}{2} + \frac{\phi}{4\beta^2}\left[2 + \frac{\beta(1-2\nu_0)}{\alpha+\beta}\right], \tag{6}$$

and

$$\alpha = (4\nu_0 - 1) + 4(1-\nu_0)\left(\frac{\kappa_0}{\kappa_1-\kappa_0} - \frac{\mu_0}{\mu_1-\mu_0}\right), \tag{7}$$

$$\beta = (3-4\nu_0) + 4(1-\nu_0)\,\frac{\mu_0}{\mu_1-\mu_0}, \tag{8}$$

where ϕ denotes the fiber volume fraction, ν_0, the Poisson's ratio of the matrix, and κ_0, κ_1 and μ_0, μ_1, the plane strain bulk and shear moduli of the matrix and fiber phases, respectively.

Following Ju and Chen (1994b), it can be shown that the averaged strain $\bar{\boldsymbol{\epsilon}}$, the uniform remote strain $\boldsymbol{\epsilon}^0$ and the averaged eigenstrain $\bar{\boldsymbol{\epsilon}}^*$ are related by (dropping the ensemble notation)

$$\bar{\boldsymbol{\epsilon}} = \boldsymbol{\epsilon}^0 + \phi\mathbf{s} : \bar{\boldsymbol{\epsilon}}^*, \tag{9}$$

where the components of the Eshelby tensor $\mathbf{s}$ (for a circular inclusion embedded in an isotropic linear elastic and infinite matrix) are

$$s_{ijkl} = \frac{1}{8(1-\nu_0)}\left\{(4\nu_0-1)\delta_{ij}\delta_{kl} + (3-4\nu_0)(\delta_{ik}\delta_{jl}+\delta_{il}\delta_{jk})\right\}, \quad i,j,k,l = 1,2. \tag{10}$$

See Mura (1987), and Ju and Zhang (1998) for more details. Therefore, we arrive at

$$\bar{\boldsymbol{\epsilon}}^* = [\Gamma\cdot(-\mathbf{A}-\mathbf{s}+\phi\mathbf{s}\cdot\Gamma)^{-1}] : \bar{\boldsymbol{\epsilon}}, \tag{11}$$

where the fourth-rank tensor $\mathbf{A}$ is defined as

$$\mathbf{A} \equiv [\mathbf{C}_1 - \mathbf{C}_0]^{-1}\cdot\mathbf{C}_0. \tag{12}$$

2.2. Effective elastic moduli of two-phase composites with circular fibers

The effective transverse elastic moduli of two-phase composites containing unidirectionally aligned, randomly located *identical* elastic circular fibers were derived by Ju and Zhang (1998) as follows

$$\mathbf{C}_* = \mathbf{C}_0\cdot\{\mathbf{I} - \phi\Gamma\cdot(-\mathbf{A}-\mathbf{s}+\phi\mathbf{s}\cdot\Gamma)^{-1}\}. \tag{13}$$

Effective plane-strain bulk modulus κ_* and shear modulus μ_* can be *explicitly* evaluated as

$$\kappa^* = \kappa_0\left\{1 + \frac{8\phi(1-\nu_0)(\gamma_1+\gamma_2)}{(\alpha+\beta) - 4\phi(\gamma_1+\gamma_2)}\right\}, \tag{14}$$

$$\mu_{\mathrm{T}}^* = \mu_0\left\{1 + \frac{8\phi(1-\nu_0)\gamma_2}{\beta - 2(3-4\nu_0)\phi\gamma_2}\right\}. \tag{15}$$

Eqs. (14) and (15) are valid for any arbitrary two-point isotropic "radial distribution function"; cf. Ju and Zhang (1998, p. 949), Verlet and Weis (1972), and Hansen and McDonald (1986). In addition, the effective transverse Young's modulus E_{T}^* and Poisson's ratio ν_{T}^* of a fiber composite are obtained through the following relations:

$$E_{\mathrm{T}}^{*}=\frac{4\kappa^{*}\mu_{\mathrm{T}}^{*}}{\kappa^{*}+\psi\mu_{\mathrm{T}}^{*}}, \tag{16}$$

$$v_{\mathrm{T}}^{*}=\frac{\kappa^{*}-\psi\mu_{\mathrm{T}}^{*}}{\kappa^{*}+\mu_{\mathrm{T}}^{*}}, \tag{17}$$

where

$$\psi=1+\frac{4v_{\mathrm{A}}^{*2}\kappa^{*}}{E_{\mathrm{A}}^{*}}. \tag{18}$$

The effective axial Young's modulus E_{A}^{*} and the effective axial Poisson's ratio v_{A}^{*} are available from Hashin (1972)

$$E_{\mathrm{A}}^{*}=E_0\phi_0+E_1\phi+\frac{4\phi\phi_0(v_1-v_0)^2}{\frac{\phi}{\kappa_0}+\frac{\phi_0}{\kappa_1}+\frac{1}{\mu_0}}, \tag{19}$$

$$v_{\mathrm{A}}^{*}=v_0\phi_0+v_1\phi+\frac{\phi\phi_0(v_1-v_0)\left(\frac{1}{\kappa_0}-\frac{1}{\kappa_1}\right)}{\frac{\phi}{\kappa_0}+\frac{\phi_0}{\kappa_1}+\frac{1}{\mu_0}}, \tag{20}$$

where $\phi_0\equiv 1-\phi$.

3. Effective elastoplastic behavior of two-phase fiber-reinforced ductile matrix composites

3.1. Basic consideration

In this section, we consider two-phase composites consisting of elastic cylindrical fibers (with bulk and shear moduli κ_1 and μ_1, respectively) unidirectionally aligned in an elastoplastic matrix (with elastic bulk and shear moduli κ_0 and μ_0, respectively). We employ the commonly used von Mises yield criterion with an isotropic hardening law for simplicity. Extension to general yield criterion and general hardening law can be derived similarly. Therefore, the stress $\boldsymbol{\sigma}$ and the equivalent plastic strain $\bar{e}^{\mathrm{p}}$ must satisfy the following yield condition at any matrix point:

$$F(\boldsymbol{\sigma},\bar{e}^{\mathrm{p}})=\sqrt{H(\boldsymbol{\sigma})}-K(\bar{e}^{\mathrm{p}})\leqslant 0. \tag{21}$$

Here, $K(\bar{e}^{\mathrm{p}})$ is the isotropic hardening function of the matrix-only material. Extension can be made to accommodate kinematic hardening law. The stress tensor $\boldsymbol{\sigma}$ for the current plane-strain problem reads

$$\boldsymbol{\sigma}=\begin{bmatrix}\sigma_{11} & \sigma_{12} & 0\\ \sigma_{21} & \sigma_{22} & 0\\ 0 & 0 & \sigma_{33}\end{bmatrix} \tag{22}$$

and

$$\sigma_{33}=v_{\mathrm{A}}^{*}(\sigma_{11}+\sigma_{22}). \tag{23}$$

Moreover, we have $H(\boldsymbol{\sigma})\equiv\boldsymbol{\sigma}:\mathbf{I}_{\mathrm{d}}:\boldsymbol{\sigma}$, where $\mathbf{I}_{\mathrm{d}}$ signifies the *deviatoric* part of the fourth-rank identity tensor $\mathbf{I}$; i.e.,

$$\mathbf{I}_{\mathrm{d}}\equiv\mathbf{I}-\tfrac{1}{3}\mathbf{1}\otimes\mathbf{1}, \tag{24}$$

where **1** is the second-rank identity tensor. Equivalently, we write $H(\sigma_{ij}) = H(s_{ij}) = s_{ij}s_{ij}$, where s_{ij} defines the second-rank deviatoric stress tensor; i.e., $s_{ij} \equiv \sigma_{ij} - 1/3\sigma_{kk}\delta_{ij}$. It is noted that $H(s_{ij})$ defines the square of the deviatoric stress norm.

The total strain $\boldsymbol{\epsilon}$ can be decomposed into two parts:

$$\boldsymbol{\epsilon} = \boldsymbol{\epsilon}^{\mathrm{e}} + \boldsymbol{\epsilon}^{\mathrm{p}} \tag{25}$$

where $\boldsymbol{\epsilon}^{\mathrm{e}}$ is the elastic strain of the matrix and fibers, and $\boldsymbol{\epsilon}^{\mathrm{p}}$ is the stress-free plastic strain in the plastic matrix only. Following Ju and Tseng (1996), we shall derive the *ensemble averaged* yield criterion for the two-phase composites. Accordingly, we adopt a technique which approximately accounts for the *pairwise interaction* among fibers while collecting the local stress perturbations in the plastic matrix. Therefore, we achieve the complete *second-order* elastoplastic formulation for two-phase FRDMCs.

3.2. A second-order formulation accounting for fiber interaction effects

In this paper, we consider *small strains* and therefore the statistical microstructure of fibers embedded in a ductile matrix remains essentially unchanged. The microstructure is therefore assumed to be statistically homogeneous and transversely isotropic with a constant fiber volume fraction during the deformation process. Furthermore, fibers are considered as elastic cylinders with uniform size.

Similar to Ju and Chen (1994a), $H(\mathbf{x}|\mathscr{G})$ denotes the square of the "current stress norm" at a local point $\mathbf{x}$ for a given fiber configuration $\mathscr{G}$. Clearly, there is no plastic strain in the elastic fibers. Therefore, $H(\mathbf{x}|\mathscr{G})$ can be expressed as

$$H(\mathbf{x}|\mathscr{G}) = \begin{cases} \boldsymbol{\sigma}(\mathbf{x}|\mathscr{G}) : \mathbf{I}_{\mathrm{d}} : \boldsymbol{\sigma}(\mathbf{x}|\mathscr{G}) & \text{if } \mathbf{x} \text{ in the matrix,} \\ 0, & \text{otherwise.} \end{cases} \tag{26}$$

Let $P(\mathscr{G})$ denote the probability density function for finding the fiber configuration $\mathscr{G}$ in the composite. Further, $\langle H \rangle_m(\mathbf{x})$ defines the ensemble average of $H(\mathbf{x}|\mathscr{G})$ over all possible realizations, where $\mathbf{x}$ is in the matrix phase:

$$\langle H \rangle_m(\mathbf{x}) = H^0 + \int_{\mathscr{G}} \{H(\mathbf{x}|\mathscr{G}) - H^0\} P(\mathscr{G})\, \mathrm{d}\mathscr{G}. \tag{27}$$

Here H^0 is the square of the far-field deviatoric stress norm in the matrix:

$$H^0 = \boldsymbol{\sigma}^0 : \mathbf{I}_{\mathrm{d}} : \boldsymbol{\sigma}^0. \tag{28}$$

In addition, the total stress at any point $\mathbf{x}$ in the matrix is the superposition of the far-field stress $\boldsymbol{\sigma}^0$ and the perturbed stress $\boldsymbol{\sigma}'$ due to the presence of the fibers:

$$\boldsymbol{\sigma}(\mathbf{x}) = \boldsymbol{\sigma}^0 + \boldsymbol{\sigma}'(\mathbf{x}), \tag{29}$$

where $\boldsymbol{\sigma}^0$ and $\boldsymbol{\sigma}'$ are defined as

$$\boldsymbol{\sigma}^0 \equiv \mathbf{C}_0 : \boldsymbol{\epsilon}^0, \tag{30}$$

and

$$\boldsymbol{\sigma}'(\mathbf{x}) \equiv \mathbf{C}_0 : \int_A \mathbf{G}(\mathbf{x} - \mathbf{x}') : \boldsymbol{\epsilon}^*(\mathbf{x}')\, \mathrm{d}\mathbf{x}'. \tag{31}$$

Here, $\boldsymbol{\epsilon}^0$ is the elastic strain field induced by the far-field loading, $\boldsymbol{\epsilon}^*$ denotes the *elastic* eigenstrain in the fiber phase, $\mathbf{C}_0$ denotes the fourth-rank elasticity tensor of the matrix, and A is the statistically representative area element (infinitely large compared with the cross-sectional area of a fiber and *without* any

prescribed displacement boundary conditions along infinite exterior boundaries). In indicial notation, the components of the fourth-rank tensor $\mathbf{G}$ take the form (cf. Mura, 1987, p. 25; Ju and Zhang, 1998, Eq. (4))

$$G_{ijkl}(\mathbf{x}-\mathbf{x}') = \frac{1}{4\pi(1-\nu_0)r^2}F_{ijkl}(-8,\ 2\nu_0,\ 2,\ 2-4\nu_0,\ -1+2\nu_0,\ 1-2\nu_0), \tag{32}$$

where $\mathbf{r} \equiv \mathbf{x}-\mathbf{x}'$, $r \equiv \|\mathbf{r}\|$, ν_0 is the Poisson's ratio of the matrix material and the indices i, j, k, l range from 1 to 2. The components of the fourth-rank tensor $\mathbf{F}$ – which depends on six scalar quantities B_1, B_2, B_3, B_4, B_5, B_6 – are defined by

$$\begin{aligned} F_{ijkl}(B_m) \equiv{}& B_1 n_i n_j n_k n_l + B_2(\delta_{ik}n_j n_l + \delta_{il}n_j n_k + \delta_{jk}n_i n_l + \delta_{jl}n_i n_k) + B_3\delta_{ij}n_k n_l + B_4\delta_{kl}n_i n_j + B_5\delta_{ij}\delta_{kl} \\ &+ B_6(\delta_{ik}\delta_{jl} + \delta_{il}\delta_{jk}) \end{aligned} \tag{33}$$

with the unit normal vector $\mathbf{n} \equiv \mathbf{r}/r$, index $m = 1$ to 6.

The unknown elastic eigenstrain $\boldsymbol{\epsilon}^*(\mathbf{x})$ within the fibers can be solved by the integral equation obtained on the basis of the *Eshelby's equivalence principle* (Eshelby, 1957), which guarantees that the equilibrium conditions in both the matrix and fiber phases and the boundary conditions at the fiber–matrix interfaces are satisfied exactly. The local (pointwise) result becomes

$$-\mathbf{A} : \boldsymbol{\epsilon}^*(\mathbf{x}) = \boldsymbol{\epsilon}^0 + \int_A \mathbf{G}(\mathbf{x}-\mathbf{x}') : \boldsymbol{\epsilon}^*(\mathbf{x}')\,\mathrm{d}\mathbf{x}', \tag{34}$$

where the fourth-rank tensor $\mathbf{A}$ is defined in Eq. (12). For the solution of the ensemble-area averaged version of Eq. (34), we refer to the derivations contained in Ju and Zhang (1998; p. 944–949).

Following Ju and Zhang (1998), the complete second-order formulation is employed to account for the *pairwise* interactions among fibers. Then a matrix point collects the perturbations from all interacting fibers. Conceptually, there exists a tiny (of the radius a) *exclusion zone* which excludes the possibility of having the center of any fiber located within the zone (Ju and Tseng, 1996). The exclusion zone will be neglected in our treatment because it is very insignificant compared with the entire (infinitely large) *statistical* averaging domain.

By using the ensemble-area averaged eigenstrain given in Eq. (3), the stress perturbation in Eq. (31) can be rewritten as

$$\boldsymbol{\sigma}'(\mathbf{x}|\mathbf{x}_1) = [\mathbf{C}_0 \cdot \bar{\mathbf{G}}(\mathbf{x}-\mathbf{x}_1)\cdot \Gamma] : \boldsymbol{\epsilon}^{*0}, \tag{35}$$

where

$$\bar{\mathbf{G}}(\mathbf{x}-\mathbf{x}_1) \equiv \int_{\Omega_1} \mathbf{G}(\mathbf{x}-\mathbf{x}')\mathrm{d}\mathbf{x}' \tag{36}$$

for $\mathbf{x} \notin \Omega_1$ in which Ω_1 is the fiber domain centered at $\mathbf{x}_1$. With the help of Eq. (33), $\bar{\mathbf{G}}$ can be expressed as

$$\bar{\mathbf{G}}(\mathbf{r}) = \frac{1}{8(1-\nu_0)}\left(\rho^2\mathbf{H}^1 + \frac{\rho^4}{2}\mathbf{H}^2\right). \tag{37}$$

The components of $\mathbf{H}^1$ and $\mathbf{H}^2$ are defined by (Ju and Zhang, 1998)

$$\mathbf{H}^1_{ijkl}(\mathbf{x}_1-\mathbf{x}_2) \equiv 2\mathbf{F}_{ijkl}(-8,\ 2\nu_0,\ 2,\ 2-4\nu_0,\ -1+2\nu_0,\ 1-2\nu_0), \tag{38}$$

$$\mathbf{H}^2_{ijkl}(\mathbf{x}_1-\mathbf{x}_2) \equiv 2\mathbf{F}_{ijkl}(24,\ -4,\ -4,\ -4,\ 1,\ 1), \tag{39}$$

where $\mathbf{r} = \mathbf{x}-\mathbf{x}_1$, $\rho = a/r$, and a is the radius of a fiber. In addition, the elastic noninteracting eigenstrain $\boldsymbol{\epsilon}^{*0}$ (corresponding to the *single* fiber inclusion problem) is given by (Ju and Chen, 1994b,c)

$$\boldsymbol{\epsilon}^{*0} = -(\mathbf{A}+\mathbf{s})^{-1} : \boldsymbol{\epsilon}^{0}, \tag{40}$$

where $\mathbf{s}$ is the plane-strain *Eshelby's tensor* for a cylindrical inclusion, which was given in Ju and Zhang (1998). Eshelby's tensor depends on Poisson's ratio of the matrix and the shape of the cylindrical inclusion. The components of $\mathbf{s}$ for a cylindrical fiber (plane-strain) have been given in Eq. (10).

3.3. A second-order formulation of effective elastoplastic behavior of fiber-reinforced ductile matrix composites

The ensemble-average stress norm for any matrix point $\mathbf{x}$ can be calculated by collecting the current stress norm perturbed due to a fiber centered at $\mathbf{x}_1$ and averaging over all possible locations of $\mathbf{x}_1$. Therefore, we have

$$\langle H\rangle_m(\mathbf{x}) \cong H^0 + \int_{|\mathbf{x}-\mathbf{x}_1|>a} \left\{H(\mathbf{x}|\mathbf{x}_1) - H^0\right\} P(\mathbf{x}_1)\,\mathrm{d}\mathbf{x}_1 + \cdots, \tag{41}$$

where $P(\mathbf{x}_1)$ defines the probability density function for finding a fiber centered at $\mathbf{x}_1$. Here, $P(\mathbf{x}_1)$ is assumed to be statistically homogeneous, isotropic and uniform, and takes the form $P(\mathbf{x}_1) = N/A$, where N is the total number of fibers dispersed in a representative area A. Further, in view of the statistical isotropy and uniformity, Eq. (41) can be rephrased as

$$\langle H\rangle_m(\mathbf{x}) \cong H^0 + \frac{N}{A}\int_a^{\infty} r\,\mathrm{d}r \int_0^{2\pi} \left\{H(\mathbf{r}) - H^0\right\}\mathrm{d}\theta + \cdots. \tag{42}$$

With the help of the two identities Eqs. (34) and (35) in Ju and Zhang (1998) and the perturbed stress rendered in Eq. (35), we obtain the ensemble-averaged current stress norm for any matrix point:

$$\langle H\rangle_m(\mathbf{x}) = \boldsymbol{\sigma}^0 : \mathbf{T} : \boldsymbol{\sigma}^0. \tag{43}$$

The components of the positive definite fourth-rank tensor $\mathbf{T}$ are defined as

$$T_{ijkl} = T_1\delta_{ij}\delta_{kl} + T_2(\delta_{ik}\delta_{jl} + \delta_{il}\delta_{jk}), \quad i,j = 1,2 \tag{44}$$

with

$$2T_1 + 2T_2 = \frac{1}{3}(1 - 4v_{\mathrm{A}}^{*} + 4v_{\mathrm{A}}^{*2}) + 16(1-2v_0)^2\frac{(\gamma_1+\gamma_2)^2}{(\alpha+\beta)^2}\phi, \tag{45}$$

$$T_2 = \frac{1}{2} + \frac{1}{3}(10 - 16v_{\mathrm{A}}^{*} + 16v_{\mathrm{A}}^{*2})\frac{\gamma_2^2}{\beta^2}\phi \tag{46}$$

in which the fiber volume fraction ϕ is defined as $\phi \equiv \pi a^2(N/A)$, and v_{A}^{*} is the effective axial Poisson's ratio.

Following Ju and Chen (1994a), the relation between the far-field stress $\boldsymbol{\sigma}^0$ and the macroscopic stress $\bar{\boldsymbol{\sigma}}$ is given by

$$\boldsymbol{\sigma}^0 = \mathbf{P} : \bar{\boldsymbol{\sigma}}, \tag{47}$$

where the components of $\mathbf{P}$ take the form

$$P_{ijkl} = P_1\delta_{ij}\delta_{kl} + P_2(\delta_{ik}\delta_{jl} + \delta_{il}\delta_{jk}) \tag{48}$$

with

$$2P_1 + 2P_2 = \frac{1}{1+b_1\phi}, \tag{49}$$

$$P_2 = \frac{1}{2(1+b_2\phi)}, \tag{50}$$

and the coefficients b_1 and b_2 are given by

$$b_1 = 4(1-2\nu_0)\frac{\gamma_1+\gamma_2}{\alpha+\beta}, \tag{51}$$

$$b_2 = \frac{2\gamma_2}{\beta}. \tag{52}$$

Substitution of Eq. (47) into Eq. (43) then leads to the following expression for the ensemble-averaged current stress norm at a matrix point:

$$\langle H\rangle_m(\mathbf{x}) = \bar{\boldsymbol{\sigma}} : \bar{\mathbf{T}} : \bar{\boldsymbol{\sigma}}, \tag{53}$$

where the positive definite fourth-rank tensor $\bar{\mathbf{T}}$ is defined as

$$\bar{\mathbf{T}} \equiv \mathbf{P}\cdot\mathbf{T}\cdot\mathbf{P}. \tag{54}$$

After lengthy algebra, the components of $\bar{\mathbf{T}}$ are derived as

$$\bar{T}_{ijkl} = \bar{T}_1\delta_{ij}\delta_{kl} + \bar{T}_2(\delta_{ik}\delta_{jl}+\delta_{il}\delta_{jk}), \tag{55}$$

where

$$\bar{T}_1 + \bar{T}_2 = \frac{T_1+T_2}{(1+b_1\phi)^2}, \tag{56}$$

$$\bar{T}_2 = \frac{T_2}{(1+b_2\phi)^2}. \tag{57}$$

In what follows, we will present a unified formulation to represent the ensemble-area averaged yield function for the two-phase ductile matrix composite, including the special case when all inclusions become aligned cylindrical voids.

The ensemble-averaged "current stress norm" for any point $\mathbf{x}$ in a two-phase fibrous or porous composite can be defined as

$$\sqrt{\langle H\rangle(\mathbf{x})} = (1-\phi_f)\sqrt{\bar{\boldsymbol{\sigma}} : \bar{\mathbf{T}} : \bar{\boldsymbol{\sigma}}}, \tag{58}$$

where ϕ_f is defined as

$$\phi_f = \begin{cases} \phi & \text{for cylindrical fibers,} \\ 0 & \text{for cylindrical voids.} \end{cases} \tag{59}$$

Accordingly, the overall effective yield function for the two-phase FRDMCs can be proposed as

$$\bar{F} = (1-\phi_f)\sqrt{\bar{\boldsymbol{\sigma}} : \bar{\mathbf{T}} : \bar{\boldsymbol{\sigma}}} - K(\bar{e}^{\mathrm{p}}), \tag{60}$$

where $K(\bar{e}^{\mathrm{p}})$ is the isotropic hardening function for the two-phase composite. Furthermore, the effective ensemble-area averaged plastic strain rate for the FRDMCs can be written as

$$\dot{\bar{\boldsymbol{\epsilon}}}^{\mathrm{p}} = \dot{\lambda}\frac{\partial\bar{F}}{\partial\bar{\boldsymbol{\sigma}}} = (1-\phi_f)\dot{\lambda}\frac{\bar{\mathbf{T}}:\bar{\boldsymbol{\sigma}}}{\sqrt{\bar{\boldsymbol{\sigma}} : \bar{\mathbf{T}} : \bar{\boldsymbol{\sigma}}}}. \tag{61}$$

For simplicity, the overall associative flow rule is assumed here. Extension to nonassociative flow rule can be constructed in a similar fashion. The effective equivalent plastic strain rate for the composite is defined as

$$\dot{\bar{e}}^{\mathrm{p}} \equiv \sqrt{\tfrac{2}{3}\dot{\bar{\boldsymbol{\epsilon}}}^{\mathrm{p}} : \bar{\mathbf{T}}^{-1} : \dot{\bar{\boldsymbol{\epsilon}}}^{\mathrm{p}}} = \sqrt{\tfrac{2}{3}}(1-\phi_f)\dot{\lambda}. \tag{62}$$

In what follows, for simplicity, the isotropic hardening function is taken as

$$K(\bar{e}^{\mathrm{p}}) = \sqrt{\tfrac{2}{3}}\{\sigma_{\mathrm{y}} + h(\bar{e}^{\mathrm{p}})^q\} \tag{63}$$

where σ_{y} is the initial yield stress, and h and q define the linear and exponential isotropic hardening parameters, respectively, for the two-phase composite.

4. Initial yield criteria for incompressible ductile matrix containing randomly located yet aligned identical cylindrical voids

Let us consider a special problem in this section – the prediction of the *initial yield* stresses for an elastically incompressible and perfectly plastic J_2-type ductile matrix containing many randomly located yet aligned identical cylindrical voids at various volume fractions. Clearly, there is nothing inside the voids and therefore the bulk and shear moduli are zero for voids. Moreover, we have $\phi_f = 0$. Consequently, the yield criterion becomes (Eq. (60))

$$\bar{F} = \sqrt{\bar{\boldsymbol{\sigma}} : \bar{\mathbf{T}} : \bar{\boldsymbol{\sigma}}} - \sqrt{\tfrac{2}{3}}\sigma_{\mathrm{y}} \tag{64}$$

in which the averaged initial yield radius is taken as $K = \sqrt{2/3}\sigma_{\mathrm{y}}$.

Since the bulk and shear moduli of voids (κ_1 and μ_1) vanish and Poisson's ratio of the matrix (v_0) equal to $1/2$, we have $\alpha = 1$, $\beta = -1$, $(1-2v_0)/(\alpha+\beta) = -1/2$ and the following expressions for this special problem:

$$T_1 + T_2 = 2(\gamma_1 + \gamma_2)^2\phi, \tag{65}$$

$$T_2 = \tfrac{1}{2} + 2\gamma_2^2\phi, \tag{66}$$

and

$$2\gamma_1 + 2\gamma_2 = 1 + \frac{\phi}{2}, \tag{67}$$

$$\gamma_2 = \tfrac{1}{2} + \tfrac{5}{8}\phi. \tag{68}$$

Notice that the effective axial Poisson's ratio (v_{A}^*) of this porous material is $1/2$ according to Hashin's upper bound (Hashin, 1972).

The total averaged stress can be split into two parts:

$$\bar{\sigma}_{ij} = \bar{s}_{ij} + \bar{\sigma}\delta_{ij} \tag{69}$$

in which the hydrostatic stress $\bar{\sigma}$ and deviatoric stress $\bar{s}_{ij}$ are defined as

$$\bar{\sigma} \equiv \tfrac{1}{3}\bar{\sigma}_{kk} \quad \text{and} \quad \bar{s}_{ij} \equiv \bar{\sigma}_{ij} - \tfrac{1}{3}\bar{\sigma}_{kk}\delta_{ij}. \tag{70}$$

Accordingly, the initial yield criterion in Eq. (64) can be rephrased as

$$\bar{F} = 6(\bar{T}_1 + \bar{T}_2)\left(\frac{\bar{\sigma}}{\sigma_{\mathrm{y}}}\right)^2 + 2\bar{T}_2\left(\frac{\bar{s}}{\sigma_{\mathrm{y}}}\right)^2 - 1 = 0, \tag{71}$$

where the definition of the deviatoric stress norm is

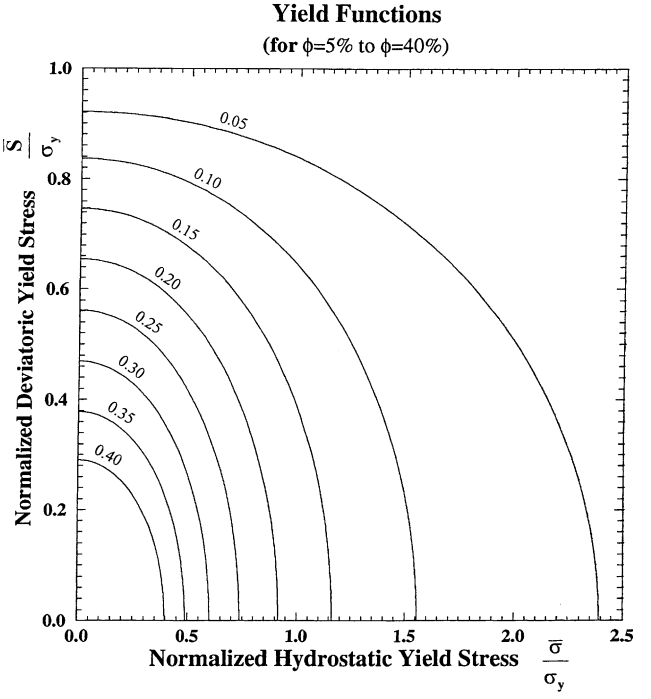

Fig. 1. The normalized initial yield surfaces for void volume fractions ϕ varying from 5% to 40%.

$$\bar{s} \equiv \sqrt{\tfrac{3}{2}\bar{s}_{ij}\bar{s}_{ij}}. \tag{72}$$

Eq. (71) represents an initial yield surface at a specified void volume fraction ϕ in the $\bar{\sigma}$–$\bar{s}$ space. The initial yield surfaces for void volume fractions ϕ varying from 0.05 to 0.4 are plotted in Fig. 1, which shows that the porous metal yields at a *lower* stress level as the volume fraction of voids ϕ increases.

The yield function corresponding to the noninteracting formulation (inter-void interaction not considered at all) can be easily derived by the following operations (cf. Ju and Zhang, 1998):

$$\gamma_1 \to 0 \quad \text{and} \quad \gamma_2 \to \tfrac{1}{2}. \tag{73}$$

Therefore, Eq. (71) is simplified as

$$\bar{F} = \frac{3\phi}{1+\phi}\left(\frac{\bar{\sigma}}{\sigma_y}\right)^2 + \left(\frac{\bar{s}}{\sigma_y}\right)^2 - \frac{(1-\phi)^2}{1+\phi} = 0 \tag{74}$$

for the noninteracting formulation.

Fig. 2 shows the comparison between the (second-order) interacting and the (first-order) noninteracting formulations in the predictions of initial yield surfaces for different void volume fractions ϕ. It is observed that the yield surfaces are larger for the noninteracting predictions. It is noted that our noninteracting formulation does account for the far-field fiber or void interactions, but not the near-field interactions.

In addition, if the applied loading becomes purely *hydrostatic*, then Eqs. (71) and (74) reduce to

$$\text{Interacting}: \quad \frac{\bar{\sigma}}{\sigma_y} = \frac{1-\phi-\frac{\phi^2}{2}}{\sqrt{3\phi\left(1+\frac{\phi}{2}\right)}}, \tag{75}$$

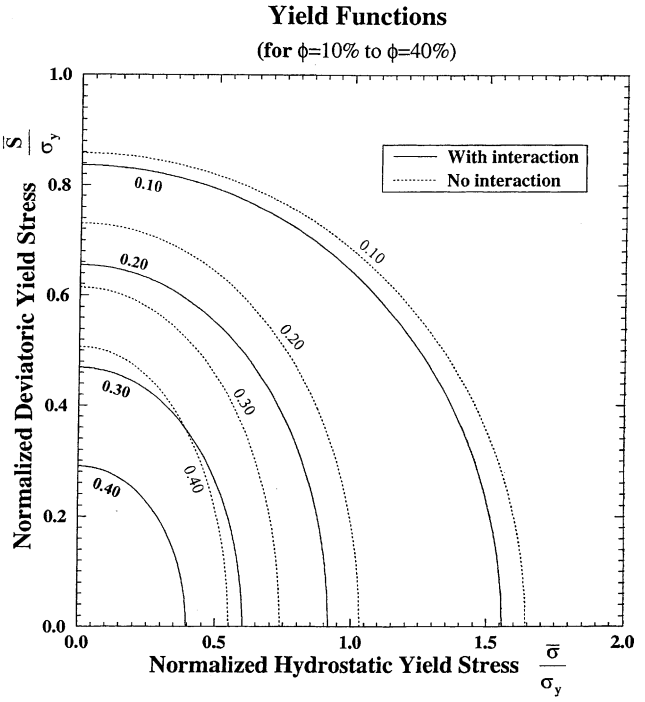

Fig. 2. Comparison of the normalized initial yield surfaces predicted by the noninteracting and the interacting formulations for void volume fractions ϕ varying from 10% to 40%.

$$\text{Noninteracting}: \quad \frac{\bar{\sigma}}{\sigma_y} = \frac{1-\phi}{\sqrt{3\phi}}. \tag{76}$$

Fig. 3 displays the normalized initial yield stresses corresponding to different void volume fractions ϕ for the noninteracting and interacting formulations under purely hydrostatic loading.

Similarly, for the purely *deviatoric* loading, the initial yield criteria become

$$\text{Interacting}: \quad \frac{\bar{s}}{\sigma_y} = \frac{1-\phi-\frac{5}{4}\phi^2}{\sqrt{1+\left(1+\frac{5}{4}\phi\right)^2\phi}}, \tag{77}$$

$$\text{Noninteracting}: \quad \frac{\bar{s}}{\sigma_y} = \frac{1-\phi}{\sqrt{1+\phi}}. \tag{78}$$

The normalized initial yield stresses are rendered in Fig. 4 for different void volume fractions ϕ corresponding to the noninteracting and interacting formulations for purely deviatoric loading.

With the pairwise void interactions accounted for, Eq. (64) can also be expressed as the ensemble-averaged stresses; namely,

$$(\bar{T}_1 + 2\bar{T}_2)\left[\bar{\sigma}_{11}^2 + \bar{\sigma}_{22}^2\right] + 2\bar{T}_1\bar{\sigma}_{11}\bar{\sigma}_{22} + 4\bar{T}_2\bar{\sigma}_{12}^2 = \tfrac{2}{3}\sigma_y^2. \tag{79}$$

For the case of the transverse biaxial loading in the x_1 and x_2-direction, only $\bar{\sigma}_{11}$ and $\bar{\sigma}_{22}$ exist. Accordingly, Eq. (79) transforms to

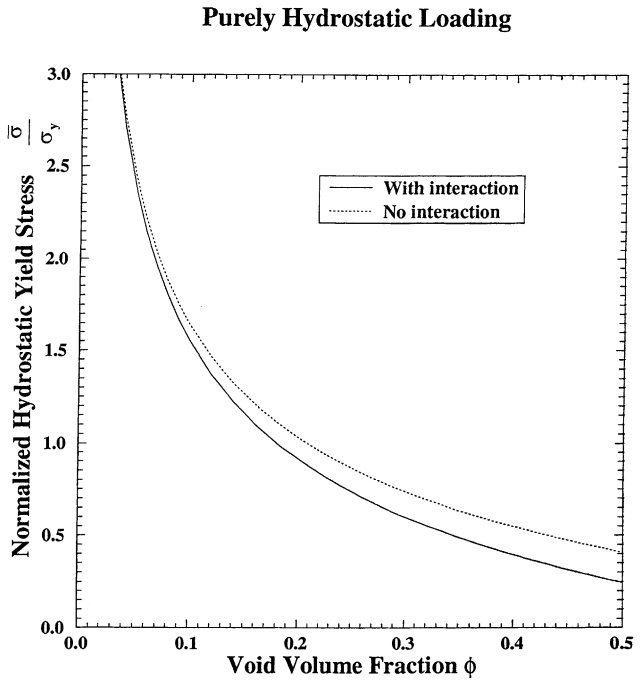

Fig. 3. Comparison of the normalized yield stresses vs. void volume fractions ϕ between the noninteracting and interacting formulations for purely hydrostatic loading.

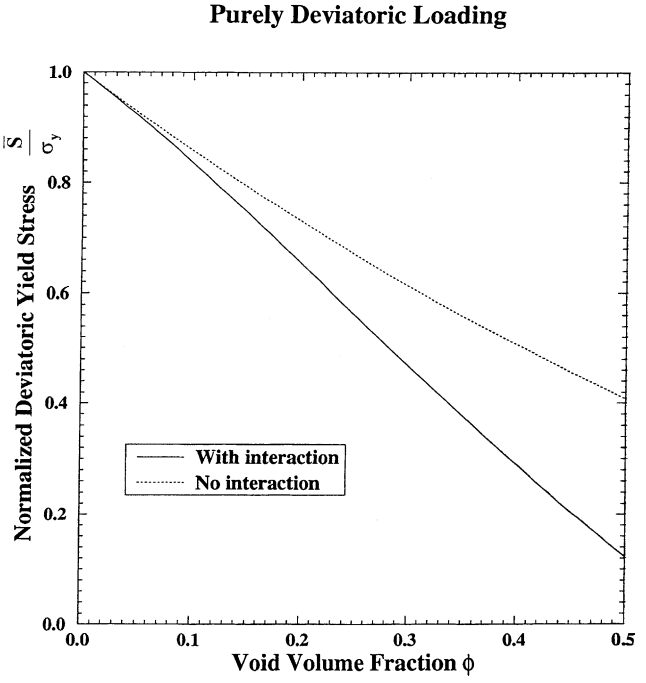

Fig. 4. Comparison of the normalized yield stresses vs. void volume fractions ϕ between the noninteracting and interacting formulations for purely deviatoric loading.

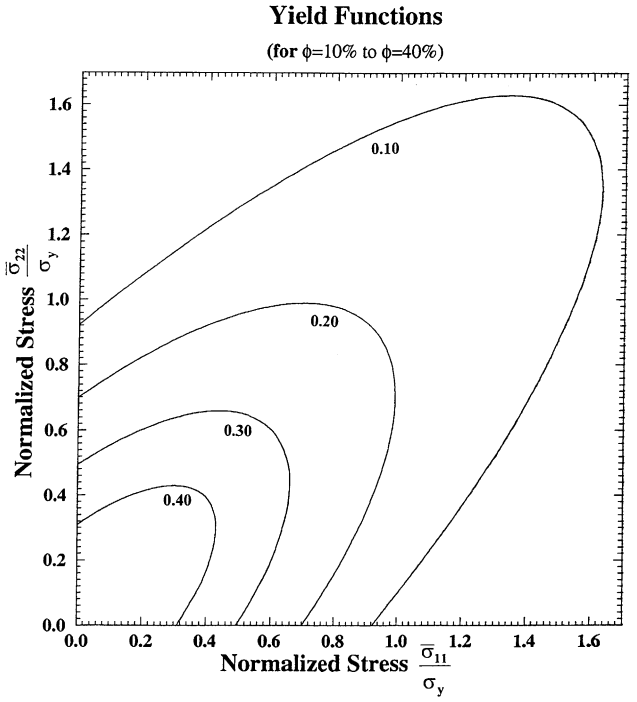

Fig. 5. The normalized initial yield surfaces under transverse biaxial loading $\bar{\sigma}_{11}$ and $\bar{\sigma}_{22}$ for void volume fractions ϕ varying from 10% to 40%.

$$(\bar{T}_1 + 2\bar{T}_2)\left[\left(\frac{\bar{\sigma}_{11}}{\sigma_y}\right)^2 + \left(\frac{\bar{\sigma}_{22}}{\sigma_y}\right)^2\right] + 2\bar{T}_1\frac{\bar{\sigma}_{11}}{\sigma_y}\frac{\bar{\sigma}_{22}}{\sigma_y} = \frac{2}{3}. \tag{80}$$

Moreover, for the case of combined uniaxial loading along the x_1-axis and the transverse torsion in x_1–x_2 plane, the initial yield surface in terms of $\bar{\sigma}_{11}$ and $\bar{\sigma}_{12}$ reads

$$(\bar{T}_1 + 2\bar{T}_2)\left(\frac{\bar{\sigma}_{11}}{\sigma_y}\right)^2 + 4\bar{T}_2\left(\frac{\bar{\sigma}_{12}}{\sigma_y}\right)^2 = \frac{2}{3}. \tag{81}$$

The families of initial yield surfaces are featured in Figs. 5 and 6, respectively, for the normalized stresses corresponding to the above two special cases. It is observed that the ellipses in Fig. 5 are oriented along the 45° direction due to the symmetry in $\bar{\sigma}_{11}$ and $\bar{\sigma}_{22}$.

5. Transverse elastoplastic behavior for fiber-reinforced ductile matrix composites

To illustrate the proposed micromechanics-based elastoplastic constitutive model for FRDMCs, let us consider two special plane-strain transverse loading conditions.

5.1. Plane-strain uniaxial loading

For the plane-strain, transverse, uniaxial loading along the x_1-direction, the applied macroscopic stress $\bar{\boldsymbol{\sigma}}$ can be written as

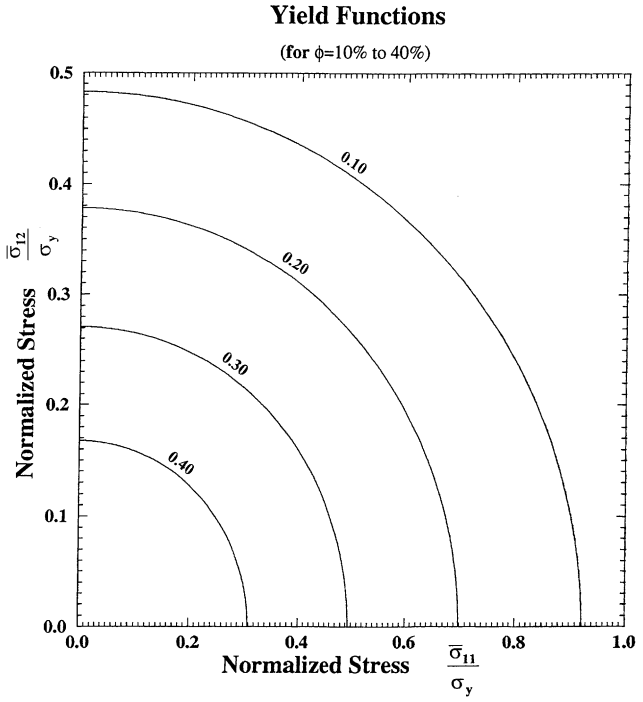

Fig. 6. The normalized initial yield surfaces under combined uniaxial loading $\bar{\sigma}_{11}$ and transverse shear $\bar{\sigma}_{12}$ for void volume fractions ϕ varying from 10% to 40%.

$$\bar{\sigma}_{11} > 0, \qquad \bar{\sigma}_{33} = v_{\mathrm{A}}^{*}\bar{\sigma}_{11}, \quad \text{all other } \bar{\sigma}_{ij} = 0. \tag{82}$$

With the help of Eqs. (63) and (82), the overall yield function becomes

$$\bar{F}(\bar{\sigma}_{11}, \bar{e}^{\mathrm{p}}) = (1-\phi)\sqrt{(\bar{T}_1 + 2\bar{T}_2)}\bar{\sigma}_{11} - \sqrt{\tfrac{2}{3}}\{\sigma_{\mathrm{y}} + h(\bar{e}^{\mathrm{p}})^q\}. \tag{83}$$

The macroscopic incremental plastic strain rate defined by Eq. (61) takes the form

$$\Delta\bar{\boldsymbol{\epsilon}}^{\mathrm{p}} = (1-\phi)\frac{\Delta\lambda}{\sqrt{(\bar{T}_1 + 2\bar{T}_2)}}\begin{bmatrix} \bar{T}_1 + 2\bar{T}_2 & 0 \\ 0 & \bar{T}_1 \end{bmatrix} \tag{84}$$

for any stress beyond the initial yielding. Similarly, the incremental equivalent plastic strain can be expressed as

$$\Delta\bar{e}^{\mathrm{p}} = \sqrt{\tfrac{2}{3}}(1-\phi)\Delta\lambda. \tag{85}$$

From the linear theory of elasticity, the macroscopic incremental elastic strain reads

$$\Delta\bar{\boldsymbol{\epsilon}}^{\mathrm{e}} = \begin{bmatrix} E_{\mathrm{A}}^{*} - E_{\mathrm{T}}^{*}v_{\mathrm{A}}^{*2} & 0 \\ 0 & -E_{\mathrm{A}}^{*}v_{\mathrm{T}}^{*} - E_{\mathrm{T}}^{*}v_{\mathrm{A}}^{*2} \end{bmatrix}\frac{\Delta\bar{\sigma}_{11}}{E_{\mathrm{T}}^{*}E_{\mathrm{A}}^{*}}. \tag{86}$$

For the *monotonic* plane-strain uniaxial loading, the overall stress–strain relation can be solved by integrating Eqs. (84) and (86) as follows:

$$\bar{\boldsymbol{\epsilon}} = \begin{bmatrix} E_{\mathrm{A}}^{*} - E_{\mathrm{T}}^{*} v_{\mathrm{A}}^{*2} & 0 \\ 0 & -E_{\mathrm{A}}^{*} v_{\mathrm{T}}^{*} - E_{\mathrm{T}}^{*} v_{\mathrm{A}}^{*2} \end{bmatrix} \frac{\bar{\sigma}_{11}}{E_{\mathrm{T}}^{*} E_{\mathrm{A}}^{*}} + (1-\phi) \frac{\lambda}{\sqrt{(\bar{T}_1 + 2\bar{T}_2)}} \begin{bmatrix} \bar{T}_1 + 2\bar{T}_2 & 0 \\ 0 & \bar{T}_1 \end{bmatrix}, \tag{87}$$

where the positive parameter λ is equal to $\sum \Delta\lambda$. By enforcing the plastic consistency condition $\bar{F} = 0$, λ can be calculated as

$$\lambda = \frac{1}{\sqrt{\frac{2}{3}}(1-\phi)} \left[\frac{(1-\phi)\sqrt{\frac{3}{2}(\bar{T}_1 + 2\bar{T}_2)}\sigma_{11} - \sigma_{\mathrm{y}}}{h} \right]^{1/q}. \tag{88}$$

To illustrate the capability of the proposed formulation, we compare our analytical prediction with the experimental data. These experimental data came from the unpublished results of an Air Force Materials Laboratory program conducted by the General Dynamics Corporation, Fort Worth Division, and quoted by Adams (1970), Zhao and Weng (1990b), DeBotton and Ponte Castañeda (1993) and other researchers. Among these experiments, three sets of test data were obtained for the 2024 aluminum alloy reinforced with unidirectionally aligned boron fibers (with 34% in fiber volume fraction) under the transverse uniaxial tensile loading. The elastic material moduli for the matrix and fiber, respectively, are

$$E_0 = 8100 \text{ ksi } (55.85 \text{ GPa}), \qquad v_0 = 0.32 \quad \text{for the 2024 aluminum alloy,}$$

and

$$E_1 = 55,000 \text{ ksi } (379.23 \text{ GPa}), \qquad v_1 = 0.20 \quad \text{for the boron fiber.}$$

In addition, the tensile stress–strain curve for the 2024 aluminum alloy (matrix) was also recorded experimentally. In order to obtain the plastic parameters σ_{y}, h and q for the matrix, we first perform the parameter estimation of the tensile stress–strain curve for the 2024 aluminum alloy. The resulting optimal values are

$$\sigma_{\mathrm{y}} = 11.5 \text{ ksi } (79.29 \text{ MPa}), \qquad h = 120 \text{ ksi } (827.4 \text{ MPa}), \qquad \text{and} \quad q = 0.6.$$

Fig. 7 displays the comparison between the experimental data (three tests) from the general dynamics and our analytical prediction for $\phi = 34\%$. The elastic response is based on the interacting micromechanical formulation of Ju and Zhang (1998). It is clear that our prediction agree very well with the elastic and initial yielding behavior. Shortly after the yield point, the composite exhibits a sudden change in the slope of experimental data, followed by long flat response up to the ultimate failure of the test specimens. This phenomenon is mainly due to the progressive interfacial debonding between the fibers and the matrix. Therefore, we need to incorporate a micromechanical damage model into our elastoplastic framework in order to account for the stress–strain behavior above the strain level of 0.15%.

Fig. 8 exhibits the predictions of the transverse stress–strain relationships $\bar{\sigma}_{11}$ vs. $\bar{\epsilon}_{11}$ (under the uniaxial tensile loading $\bar{\sigma}_{11}$) of the above 2024 Al–B composites with different fiber volume fractions varying from 10% to 40%.

As a special case, the transverse stress–strain behavior of the 2024 aluminum containing unidirectionally aligned cylindrical voids is also studied in the same manner for different void volume fractions. From Fig. 9, it is observed that both the elastic moduli and the initial yield stresses decrease with increasing void volume fractions.

5.2. Plane-strain biaxial loading

For the plane-strain transverse biaxial loading, the applied macroscopic stress $\bar{\boldsymbol{\sigma}}$ can be written as

$$\bar{\sigma}_{11} > 0, \qquad \bar{\sigma}_{22} = R\bar{\sigma}_{11}, \qquad \bar{\sigma}_{33} = v_{\mathrm{A}}^{*}(\bar{\sigma}_{11} + \bar{\sigma}_{22}), \quad \text{all other } \bar{\sigma}_{ij} = 0. \tag{89}$$

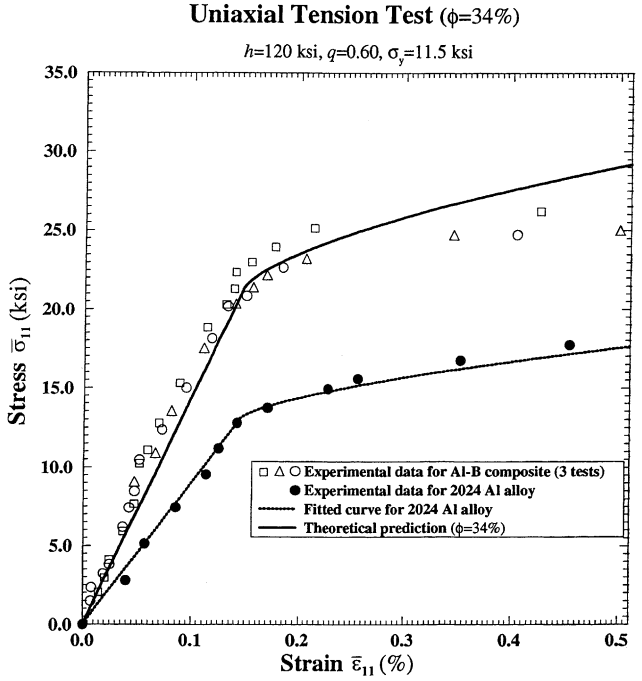

Fig. 7. Overall transverse stress–strain relationship $\bar{\sigma}_{11}$ vs. $\bar{\epsilon}_{11}$ of the 2024 Al–B composite for $\phi = 34\%$. The solid line corresponds to the present prediction and the circles, squares and triangles correspond to experimental data (General Dynamics, Fort Worth Division).

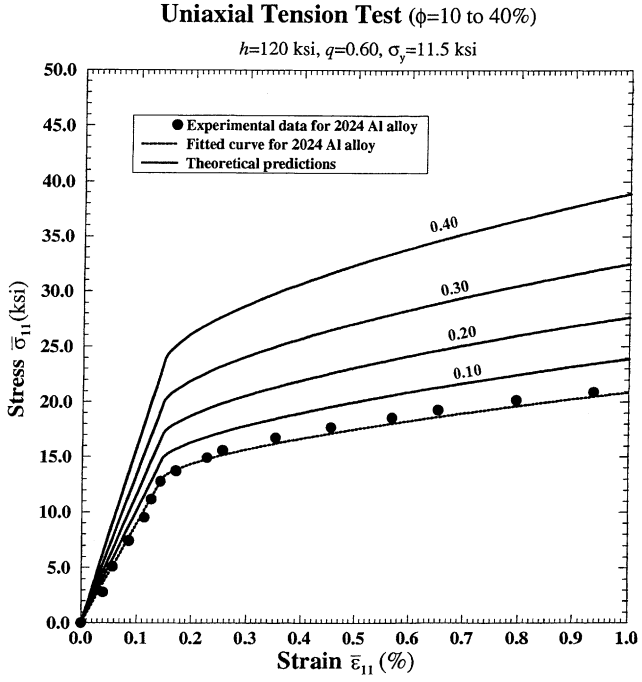

Fig. 8. Overall transverse stress–strain relationships $\bar{\sigma}_{11}$ vs. $\bar{\epsilon}_{11}$ of the 2024 Al–B composites for various $\phi = 10\%$, 20%, 30%, 40%.

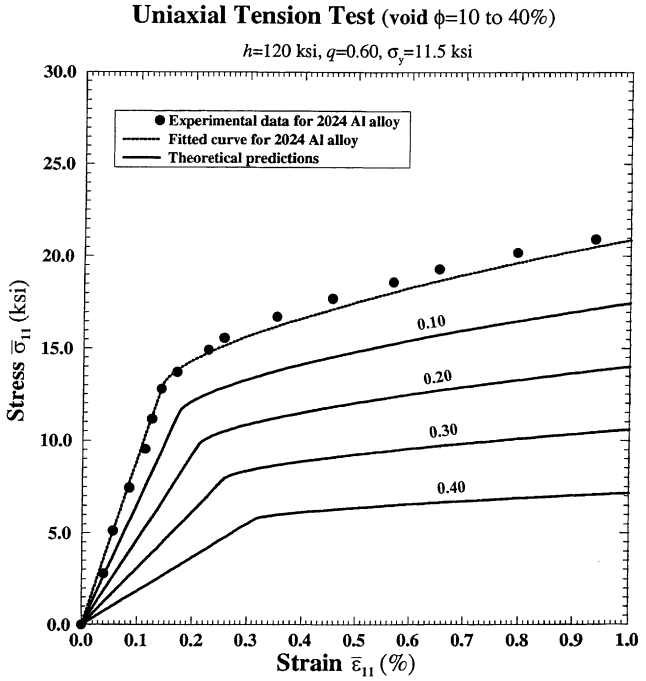

Fig. 9. Overall transverse stress–strain relationships $\bar{\sigma}_{11}$ vs. $\bar{\epsilon}_{11}$ of the 2024 aluminum alloy containing unidirectionally aligned voids for various void volume fractions $\phi = 10\%, 20\%, 30\%, 40\%$.

Here, the stress ratio R is a constant. Specifically, if $R=0$, the above plane-strain uniaxial loading case will be recovered. Substituting Eqs. (63) and (89) into Eq. (60), the effective yield function for the plane-strain biaxial loading becomes

$$\bar{F}(\bar{\sigma}_{11}, \bar{e}^{\mathrm{p}}) = (1-\phi)\Phi(R)\bar{\sigma}_{11} - \sqrt{\tfrac{2}{3}}\left\{\sigma_{\mathrm{y}} + h(\bar{e}^{\mathrm{p}})^{q}\right\}, \tag{90}$$

where

$$\Phi(R) = \sqrt{\bar{T}_1(1+R)^2 + 2\bar{T}_2(1+R^2)}. \tag{91}$$

Furthermore, the macroscopic incremental plastic strain rate defined by Eq. (61) takes the form

$$\Delta\bar{\epsilon}^{\mathrm{p}} = (1-\phi)\frac{\Delta\lambda}{\Phi(R)}\begin{bmatrix} (1+R)\bar{T}_1 + 2\bar{T}_2 & 0 \\ 0 & (1+R)\bar{T}_1 + 2R\bar{T}_2 \end{bmatrix} \tag{92}$$

for any stress beyond the initial yielding. Similarly, the incremental equivalent plastic strain can be expressed as

$$\Delta\bar{e}^{\mathrm{p}} = \sqrt{\tfrac{2}{3}}(1-\phi)\Delta\lambda. \tag{93}$$

From the linear elasticity, the macroscopic incremental elastic strain is

$$\Delta\bar{\epsilon}^{\mathrm{e}} = \begin{bmatrix} E^*_{\mathrm{A}}(1-v^*_{\mathrm{T}}R) - E^*_{\mathrm{T}}v^{*2}_{\mathrm{A}}(1+R) & 0 \\ 0 & (R-v^*_{\mathrm{T}})E^*_{\mathrm{A}} - E^*_{\mathrm{T}}v^{*2}_{\mathrm{A}}(1+R) \end{bmatrix} \frac{\Delta\bar{\sigma}_{11}}{E^*_{\mathrm{T}}E^*_{\mathrm{A}}}. \tag{94}$$

For the *monotonic* plane-strain biaxial loading, the overall stress–strain relation can be derived by integrating Eqs. (92) and (94) as follows:

$$\bar{\boldsymbol{\epsilon}} = \begin{bmatrix} E_{\mathrm{A}}^{*}(1-v_{\mathrm{T}}^{*}R) - E_{\mathrm{T}}^{*}v_{\mathrm{A}}^{*2}(1+R) & 0 \\ 0 & (R-v_{\mathrm{T}}^{*})E_{\mathrm{A}}^{*} - E_{\mathrm{T}}^{*}v_{\mathrm{A}}^{*2}(1+R) \end{bmatrix} \frac{\bar{\sigma}_{11}}{E_{\mathrm{T}}^{*}E_{\mathrm{A}}^{*}} + (1-\phi) \times \frac{\lambda}{\Phi(R)} \begin{bmatrix} (1+R)\bar{T}_1 + 2\bar{T}_2 & 0 \\ 0 & (1+R)\bar{T}_1 + 2R\bar{T}_2 \end{bmatrix}. \tag{95}$$

Similar to the above procedure, the expression for λ is

$$\lambda = \frac{1}{\sqrt{\frac{2}{3}}(1-\phi)} \left[\frac{\sqrt{\frac{3}{2}}(1-\phi)\Phi(R)\sigma_{11} - \sigma_{\mathrm{y}}}{h} \right]^{1/q}. \tag{96}$$

Since no experimental data is available for the plane-strain biaxial loading, we will employ the same material properties of the boron fiber reinforced 2024 aluminum alloy as Section 5.1. Fig. 10 shows the predicted stress–strain relationships $\bar{\sigma}_{11}$ vs. $\bar{\epsilon}_{11}$ for the 2024 Al–B composite ($\phi = 34\%$) under the plane-strain biaxial loading for various R values (0, 0.2, 0.4, 0.6, 0.8, 1.0, 1.2 and 1.4). The stress–strain curves exhibit less nonlinear behavior with increasing R values until the negative strain effect occurs. Similarly, Fig. 11 renders the predictions of $\bar{\sigma}_{22}$ vs. $\bar{\epsilon}_{22}$ for different R values (0.2, 0.4, 0.6, 0.8, 1.0, 1.2 and 1.4).

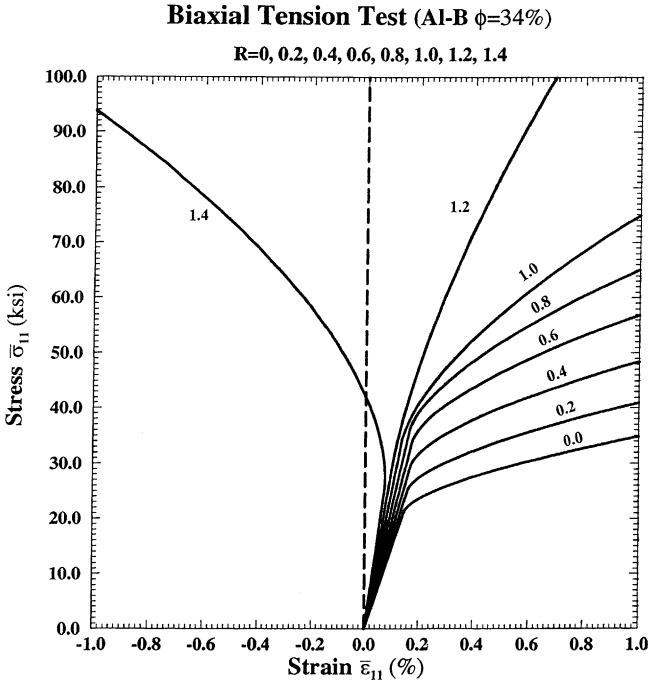

Fig. 10. Overall transverse stress–strain relationships $\bar{\sigma}_{11}$ vs. $\bar{\epsilon}_{11}$ of the 2024 Al–B composite ($\phi = 34\%$) for various R under biaxial loading.

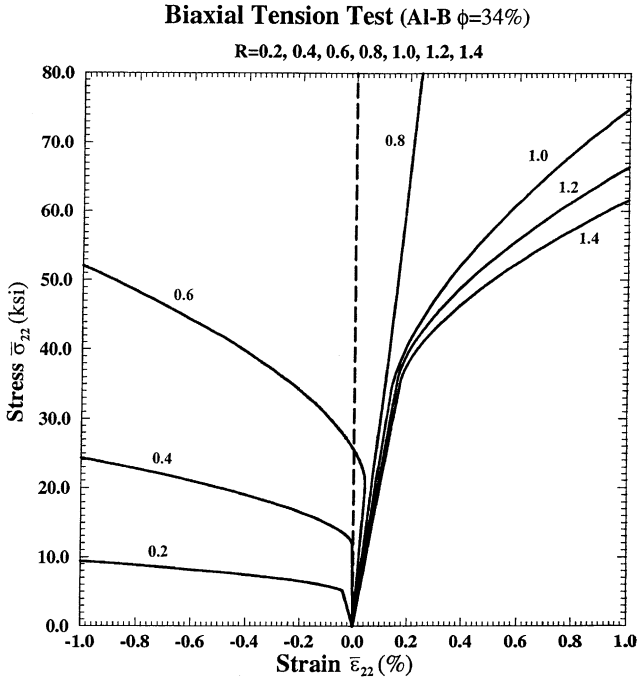

Fig. 11. Overall transverse stress–strain relationships $\bar{\sigma}_{22}$ vs. $\bar{\varepsilon}_{22}$ of the 2024 Al–B composite ($\phi = 34\%$) for various R under biaxial loading.

6. Initial yield surfaces of fiber-reinforced ductile matrix composites

For general loading conditions, the initial yield surfaces of FRDMCs can be obtained by a procedure similar to that employed in Section 4. In view of the existence of unidirectionally aligned yet randomly located fibers, the initial yield criterion reads (cf. Eq. (60))

$$\bar{F} = (1-\phi)\sqrt{\bar{\boldsymbol{\sigma}} : \bar{\mathbf{T}} : \bar{\boldsymbol{\sigma}}} - \sqrt{\tfrac{2}{3}}\sigma_y, \tag{97}$$

where the averaged initial yield radius is $K = \sqrt{2/3}\sigma_y$. After carrying out the tensor contraction in Eq. (97), we arrive at

$$(\bar{T}_1 + 2\bar{T}_2)\left[\bar{\sigma}_{11}^2 + \bar{\sigma}_{22}^2\right] + 2\bar{T}_1\bar{\sigma}_{11}\bar{\sigma}_{22} + 4\bar{T}_2\bar{\sigma}_{12}^2 = \frac{2\sigma_y^2}{3(1-\phi)^2}. \tag{98}$$

In the case of transverse biaxial loading in the x_1- and x_2-direction, only $\bar{\sigma}_{11}$ and $\bar{\sigma}_{22}$ exist. Therefore, Eq. (98) reduces to

$$(\bar{T}_1 + 2\bar{T}_2)\left[\left(\frac{\bar{\sigma}_{11}}{\sigma_y}\right)^2 + \left(\frac{\bar{\sigma}_{22}}{\sigma_y}\right)^2\right] + 2\bar{T}_1\frac{\bar{\sigma}_{11}}{\sigma_y}\frac{\bar{\sigma}_{22}}{\sigma_y} = \frac{2}{3(1-\phi)^2}. \tag{99}$$

Moreover, for the combined loading involving a tension in the x_1-axis and a transverse torsion, the initial yield surface in terms of $\bar{\sigma}_{11}$ and $\bar{\sigma}_{12}$ reads

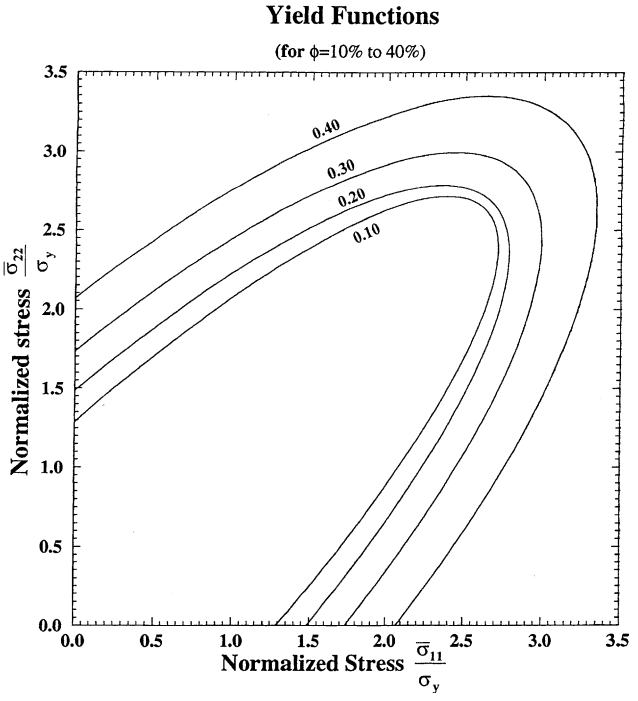

Fig. 12. The normalized initial yield surfaces under transverse biaxial loading $\bar{\sigma}_{11}$ and $\bar{\sigma}_{22}$ for the 2024 Al–B composites with various fiber volume fractions ($\phi = 10\%$, 20%, 30%, 40%).

$$(\bar{T}_1 + 2\bar{T}_2)\left(\frac{\bar{\sigma}_{11}}{\sigma_y}\right)^2 + 4\bar{T}_2\left(\frac{\bar{\sigma}_{12}}{\sigma_y}\right)^2 = \frac{2}{3(1-\phi)^2}. \tag{100}$$

The predictions of initial yield surfaces for the foregoing Al–B composites under the transverse biaxial loading are shown in Fig. 12 for various fiber volume fractions. The family of ellipses in Fig. 12 features the same symmetry as that in Fig. 5. In addition, the initial yield surfaces for the combined tensile and shear loading are depicted in Fig. 13 for different fiber volume fractions.

7. Elasto-viscoplastic behavior of fiber-reinforced ductile matrix composites

Following Simo et al. (1988), Ju (1990) and Ju and Tseng (1997), the rate constitutive equations of the generalized Duvaut–Lions viscoplasticity (Duvaut and Lions, 1972) can be formulated as

$$\dot{\bar{\boldsymbol{\epsilon}}}^{\mathrm{vp}} = \frac{1}{\eta}\mathbf{C}_*^{-1} : [\bar{\boldsymbol{\sigma}} - \bar{\bar{\boldsymbol{\sigma}}}], \tag{101}$$

$$\dot{\bar{\boldsymbol{e}}}^{\mathrm{vp}} = -\frac{1}{\eta}[\bar{\boldsymbol{e}}^{\mathrm{vp}} - \bar{\bar{\boldsymbol{e}}}^{\mathrm{p}}], \tag{102}$$

where η is the viscosity coefficient with the unit of time. Moreover, $\bar{\bar{\boldsymbol{\sigma}}}$ and $\bar{\bar{\boldsymbol{e}}}^{\mathrm{p}}$ denote the overall stress tensor and the hardening parameter, respectively, of the inviscid elastoplastic solution. $\bar{\boldsymbol{\sigma}}$ and $\bar{\boldsymbol{e}}^{\mathrm{vp}}$ define the total

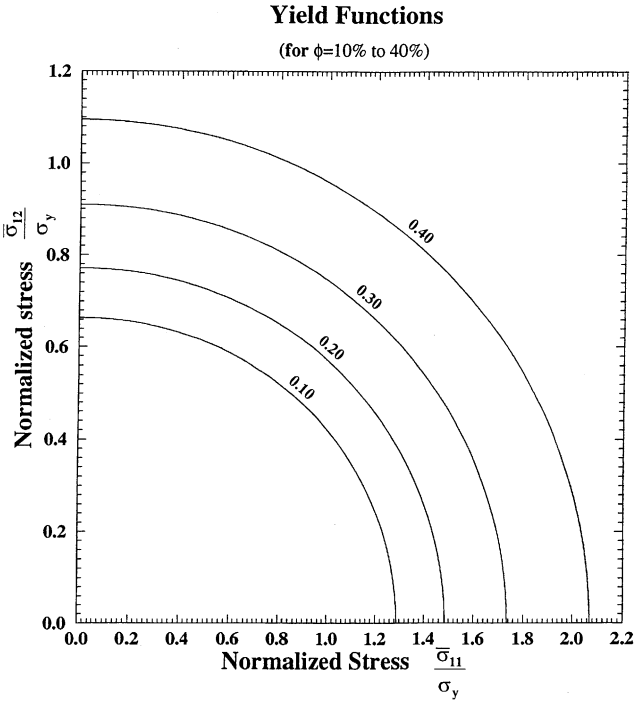

Fig. 13. The normalized initial yield surfaces under combined uniaxial loading $\bar{\sigma}_{11}$ and transverse shear $\bar{\sigma}_{12}$ for the 2024 Al–B composites with various fiber volume fractions ($\phi = 10\%$, 20%, 30%, 40%).

averaged stress and the hardening parameter, respectively, of the viscoplastic solution. In addition, $\dot{\bar{\epsilon}}^{\mathrm{vp}}$ denotes the viscoplastic strain rate tensor.

We can easily derive the discrete backward Euler algorithm for the viscoplastic problem as follows:

$$\bar{\boldsymbol{\sigma}}_{n+1} = \frac{\bar{\boldsymbol{\sigma}}^{\mathrm{tr}}_{n+1} + \frac{\Delta t_{n+1}}{\eta}\bar{\bar{\boldsymbol{\sigma}}}_{n+1}}{1 + \frac{\Delta t_{n+1}}{\eta}}, \tag{103}$$

$$\bar{\boldsymbol{e}}^{\mathrm{vp}}_{n+1} = \frac{\bar{\boldsymbol{e}}^{\mathrm{vp}}_{n} + \frac{\Delta t_{n+1}}{\eta}\bar{\bar{\boldsymbol{e}}}^{\mathrm{p}}_{n+1}}{1 + \frac{\Delta t_{n+1}}{\eta}} \tag{104}$$

in which $\bar{\boldsymbol{\sigma}}^{\mathrm{tr}}_{n+1} = \bar{\boldsymbol{\sigma}}_n + \mathbf{C}_* : \Delta\bar{\boldsymbol{\epsilon}}_{n+1}$ represents the "elastic predictor". $\Delta\bar{\boldsymbol{\epsilon}}_{n+1}$ and Δt_{n+1} denote the overall total strain increment and time step, respectively. If $\Delta t/\eta \to \infty$, then the inviscid plasticity is recovered. By contrast, if $\Delta t/\eta \to 0$, then the instantaneous elasticity is recovered. Fig. 14 provides the predictions of overall elasto-viscoplastic behavior of the above Al–B composites (fiber volume fraction 34%) under the plane-strain transverse uniaxial tension. It is noted that the overall Duvaut–Lions viscoplastic responses ($\eta = 10^{-5}$ and 10^{-4}) lie between the elastic solution ($\eta = 10^{10}$) and the inviscid plastic solution ($\eta = 10^{-10}$).

8. Conclusion

A micromechanical framework is developed in this paper to predict effective elastoplastic behavior of two-phase FRDMCs containing many unidirectionally aligned yet randomly located elastic cylindrical

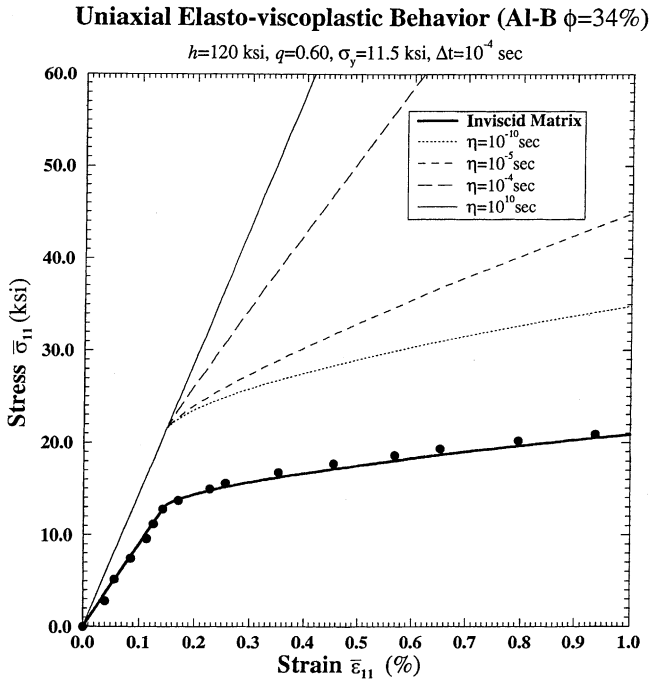

Fig. 14. Predictions of overall transverse elasto-viscoplastic behavior of the Al–B composites under uniaxial tension for different viscosity parameters η.

fibers. We have presented a complete *second-order* formulation using the uniform radial distribution function of the aligned fibers, explicit pairwise fiber interactions (for both the elastic and plastic sub-problems), and the ensemble-area averaging procedure. Subsequently, a unified formulation is proposed for both fibers and voids. The present formulation is capable of treating general plane-strain loading and unloading histories. However, the current work does not account for thermal loading, residual stress field, or cyclic fatigue loading. Furthermore, the present method is different from the existing effective medium methods developed for FRDMCs since it accommodates *explicit* inter-fiber interactions and *random* fiber distributions.

The initial yield criteria for incompressible ductile matrix containing many identical, aligned cylindrical voids is studied. The proposed method is applied to the special cases of transverse uniaxial, biaxial and combined loading to predict the transverse elastoplastic stress–strain responses. Moreover, our plane-strain uniaxial predictions are compared with the experimental data reported by Adams (1970). The overall elasto-viscoplastic behavior of FRDMCs is also explored based on the Duvaut–Lions viscoplasticity. Finally, the stress–strain relations for the Al–B composites under the transverse uniaxial tension is discussed for different viscosity coefficients η.

Further research is warranted to incorporate micromechanical damage models into our elastoplastic framework in order to characterize the progressive interfacial (complete or partial) debonding mechanism between the fibers and the matrix. Ju and Lee (2000) recently proposed a similar framework along this line for ductile matrix composites containing randomly dispersed *spherical* particles with evolutionary complete interfacial particle debonding.

In the present study, we have assumed that the quadratic functional form of the overall yield function is similar to that of the matrix material for simplicity. However, in general, this assumption may not be universal for all FRDMCs. For example, Hashin (1980) and Dvorak et al. (1988) suggested that the overall

yield function of anisotropic composites be constructed from piecewise smooth sections and not from a single smooth surface. Furthermore, more general isotropic/kinematic hardening laws and alternative nonassociative flow rule can be accommodated within the proposed framework based on available experimental data; see, e.g., Dvorak et al. (1988) for kinematic hardening law and nonassociative flow rule. These issues will be further studied in the future.

Acknowledgements

This work was sponsored by the National Science Foundation, Mechanics and Materials Program under PYI Grant MSS-9157238, and the CUREe-Kajima Phase II Research Project under Grant D950217. These supports are gratefully acknowledged.

References

Adams, D.F., 1970. Inelastic analysis of a unidirectional composite subjected to transverse normal loading. J. Comp. Mater. 4, 310–328.

Batchelor, G.K., Green, J.T., 1972. The determination of the bulk stress in a suspension of spherical particles to order c^2. J. Fluid Mech. 56, 401–427.

Chen, H.-S., Acrivos, A., 1978. The effective elastic moduli of composite materials containing spherical inclusions at non-dilute concentrations. Int. J. Solids Struct. 14, 349–364.

DeBotton, G., Ponte Castañeda, P., 1993. Elastoplastic constitutive relations for fiber-reinforced solids. Int. J. Solids Struct. 30, 1865–1890.

Duvaut, G., Lions, J.L., 1972. Les inequations en mechanique et en physique. Dunod, Paris, France (in French).

Dvorak, G.J., Bahei-El-Din, Y.A., 1987. A bimodal plasticity theory of fibrous composite materials. Acta Mech. 69, 219–241.

Dvorak, G.J., Bahei-El-Din, Y.A., Macheret, Y., Liu, C.H., 1988. An experimental study of elastic–plastic behavior of a fibrous Boron–Aluminum composite. J. Mech. Phys. Solids 36, 655–687.

Dvorak, G.J., 1991. Plasticity theories for fibrous composite materials. In: Everett, R.K., Arsenault, R.J. (Eds.), Metal Matrix Composites: Mechanisms and Properties. Academic Press, Boston.

Eshelby, J.D., 1957. The determination of the elastic field of an ellipsoidal inclusion and related problems. Proc. Roy. Soc. London Ser. A 241, 376–396.

Hansen, J.P., McDonald, I.R, 1986. Theory of Simple Liquids. Academic Press, New York.

Hashin, Z., 1972. Theory of Fiber Reinforced Materials. NASA CR-1974.

Hashin, Z., 1980. Failure criteria for unidirectional fiber composites. J. Appl. Mech. 47, 329–334.

Hashin, Z., 1983. Analysis of composite materials – a survey. J. Appl. Mech. 50, 481–505.

Hill, R., 1963. Elastic properties of reinforced solids: some theoretical principles. J. Mech. Phys. Solids 11, 357–372.

Hill, R., 1964a. Theory of mechanical properties of fiber-strengthened materials: I. Elastic behavior. J. Mech. Phys. Solids 12, 199–213.

Hill, R., 1964b. Theory of mechanical properties of fiber-strengthened materials: II. Inelastic behavior. J. Mech. Phys. Solids 12, 214–218.

Ju, J.W., 1990. Consistent tangent moduli for a class of viscoplasticity. ASCE J. Engng. Mech. 116, 1764–1779.

Ju, J.W., Chen, T.M., 1994a. Micromechanics and effective elastoplastic behavior of two-phase metal matrix composites. J. Engng. Mater. Technol. 116, 310–318.

Ju, J.W., Chen, T.M., 1994b. Micromechanics and effective moduli of elastic composites containing randomly dispersed ellipsoidal inhomogeneities. Acta Mech. 103, 103–121.

Ju, J.W., Chen, T.M., 1994c. Effective elastic moduli of two-phase composites containing randomly dispersed spherical inhomogeneities. Acta Mech. 103, 123–144.

Ju, J.W., Lee, H.K., 2000. A micromechanical damage model for effective elastoplastic behavior of ductile matrix composites considering evolutionary complete particle debonding. Comput. Meth. Appl. Mech. Engng. 183, 201–222.

Ju, J.W., Tseng, K.H., 1996. Effective elastoplastic behavior of two-phase ductile matrix composites: a micromechanical framework. Int. J. Solids Struct. 33, 4267–4291.

Ju, J.W., Tseng, K.H., 1997. Effective elastoplastic algorithms for ductile matrix composites. J. Engng. Mech. ASCE 123, 260–266.

Ju, J.W., Zhang, X.D., 1998. Micromechanics and effective transverse elastic moduli of composites with randomly located aligned circular fibers. Int. J. Solids Struct. 35, 941–960.

Lin, C.H., Salinas, D., Ito, Y.M., 1972a. Initial yield surface of a unidirectionally reinforced composites. J. Appl. Mech. 39, 321–326.
Lin, C.H., Salinas, D., Ito, Y.M., 1972b. Elastic–plastic analysis of unidirectional composites. J. Comput. Mater. 6, 48–60.
Mori, T., Tanaka, K., 1973. A average stress in a matrix and average elastic energy of materials with misfitting inclusions. Acta Mech. 21, 571–574.
Mura, T., 1987. Micromechanics of Defects in Solids, second ed. Martinus Nijhoff Publishers, Dordrechet.
Nemat-Nasser, S., Hori, M., 1993. Micromechanics: Overall Properties of Heterogeneous Materials. Elsevier, Amsterdam.
Ponte Castañeda, P., 1991. The effective mechanical properties of nonlinear isotropic composites. J. Mech. Phys. Solids 39, 45–71.
Ponte Castañeda, P., 1992. New variational principles in plasticity and their application to composite materials. J. Mech. Phys. Solids 40, 1757–1788.
Simo, J.C., Kennedy, J.G., Govindjee, S., 1988. Non-smooth multisurface plasticity and viscoplasticity. Loading/unloading conditions and numerical algorithms. Int. J. Numer. Meth. Engng. 26, 2161–2185.
Tandon, G.P., Weng, G.J., 1988. A theory of particle-reinforced plasticity. J. Appl. Mech. 55, 126–135.
Verlet, L., Weis, J.-J., 1972. Equilibrium theory of simple liquids. Phys. Rev. A 5 (2), 939–952.
Willis, J.R., 1981. Variational and related methods for the overall properties of composites. In: Yih, C.S. (Ed.), Advances in Applied Mechanics. Academic Press, New York, pp. 1–78.
Willis, J.R., 1982. Elasticity theory of composites. In: Hopkins, H.G., Sewell, M.J. (Eds.), Mechanics of Solids, the Rodney Hill 60th Anniversary Volume. Pergamon Press, New York, pp. 653–686.
Willis, J.R., Acton, J.R., 1976. The overall elastic moduli of a dilute suspension of spheres. Q. J. Mech. Appl. Math. 29, 163–177.
Zhao, Y.H., Weng, G.J., 1990a. Effective elastic moduli of ribbon-reinforced composites. J. Appl. Mech. 57, 158–167.
Zhao, Y.H., Weng, G.J., 1990b. Theory of plasticity for a class of inclusion and fiber-reinforced composites. In: Weng, G.J., Taya, M., Abe, H. (Eds.), Micromechanics and Inhomogeneity. Springer, New York, pp. 599–622.